Turbulence increases the average settling velocity of phytoplankton cells

Javier Ruiz*[†], Diego Macías[‡], and Francesc Peters[§]

*Instituto de Ciencias Marinas de Andalucía and [‡]Consejo Superior de Investigaciones Científicas, Área de Ecología, Facultad de Ciencias del Mar, Universidad de Cádiz, Campus Río San Pedro, 11510 Puerto Real, Cádiz, Spain; and [§]Institut de Ciènces del Mar, Consejo Superior de Investigaciones Científicas, Passeig Marítim de la Barceloneta 37-49, 08003 Barcelona, Catalunya, Spain

It is a well known fact that stirring keeps particles suspended in fluids. This is apparent, for instance, when shaking medicine flasks, when agitating tea deposits in a mug, or when heavy winds fill the air with dust particles. The commonplace nature of such observations makes it easy to accept that this feature will apply to any natural phenomenon as long as the flow is turbulent enough. This has been the case for phytoplankton in the surface mixed layers of lakes and oceans. The traditional view assumes that an increase in turbulence bears ecological advantages for nonmotile groups like diatoms that, otherwise, would settle in deep and unlit waters. However, this assumption has no theoretical ground, and the experimental results we present here point in the opposite direction. Phytoplankton settling velocity increases when turbulence intensifies from the low to the higher values recorded in the upper mixed layers of lakes and oceans. Consequently, turbulence does not favor phytoplankton remaining in lit waters but is rather an environmental stress that can only be avoided through morphological and/or physiological adaptations.

Phytoplankton in the upper mixed layers of lakes and oceans live in a turbulent flow regime. This circumstance may shape many features of their physiological and morphological functioning including the efficiency of nutrient assimilation (1), prey–predator interactions (2) and cell division (3). One of the key controls turbulence exerts on phytoplankton results from its effect on sedimentation rates. A compensatory role is usually assumed for turbulence, especially for nonmotile cells lacking other mechanisms to counteract their sinking from the surface to depth. However, this potential role cannot result from a direct effect of turbulence on the settling velocity of cells. The results presented in this paper clearly demonstrate that turbulence increases the settling of phytoplankton cells, regardless of the species considered and independent of turbulence-generation devices or velocity-measurement instruments. Our evidence questions the traditionally accepted notion that turbulence diminishes phytoplankton settling in the ocean.

Methods

Experimental Particles. Four phytoplankton species (*Coscinodiscus* sp., *Nitzschia* sp., *Heterocapsa* sp., and *Pleurochrysis* sp.) of different size [200-, 30-, 25-, and 18-μm equivalent spherical diameters (ESDs), respectively] and morphology were immersed in flows of various turbulent intensities, and particle settling velocities were subsequently recorded. Additional experiments were done with commercial pollen grains (*Cistacea*e, 40-μm ESD), polystyrene spheres (197-μm ESD), and decapsulated cysts of *Artemia salina* (250-μm ESD) as examples of particles in the size range of large phytoplankton and with a tendency to sink (pollen and spheres) or float (cysts).

All experiments were made with particle concentrations <20 ppm by volume, with negligible effects on the flow. It is also a low concentration to expect significant deviations from Stokes terminal velocity due to interactions between the fields generated by two falling particles (4). These deviations scale as the ratio of particle diameter to distance between particles (4). The value of the latter can be estimated as the inverse cube root of the particle concentration (<20 ppm by volume) divided by individual volume (function of particle ESD). Ratios of ESD to distance between particle of the order of 0.01 are obtained. Deviations from Stokes terminal velocities observed in our experiments are much higher (see below). Therefore, interaction between particles cannot be the exclusive origin of the results presented below. On the other hand, temperature variations were lower than one degree throughout the duration of the experiments with a negligible effect on particle velocity due to viscosity changes.

Experimental Devices. We carried out a cluster of experiments with different turbulence-generating devices and particle velocity recording techniques. These experiments were aimed at guaranteeing that the experimental output was not hindered by artifacts caused by either the devices implemented to generate the flow or by the technique used to record particle velocities. A set of experiments generated turbulence by rotating a thin cylinder within cylindrical tanks of different diameters in a Couette device type of design with optoelectronic instruments implemented for recording velocities (Fig. 1 *a* and *b*). Another set of experiments was conducted with a vertically oscillating grid immersed in a 12.9-cm-diameter cylindrical tank (Fig. 1*c*). In this case, different levels of turbulence intensity were obtained through frequency variations of the oscillating grid and velocities recorded by acoustic methods. Neither the Couette nor the grid system generated large stable structures in the flow. Therefore, the behavior of particles in the bulk flow is the result of their interaction with turbulence at small scale.

Optoelectronic: Couette device type. The annular volume between a small inner cylinder and a larger cylindrical tank, with diameters of 4 cm and 30 cm, respectively, was filled with particle-free seawater and inoculated with a phytoplankton culture. The small cylinder was spun at angular velocities (Ω) between 1.4 and 6.3 rad per s to produce different levels of turbulence intensity. Reynolds (*Re*) and Taylor (*T*) numbers characterize the level of flow instability within Couette devices (5). These numbers can be calculated as (5)

$$\mathrm{Re} = \Omega r d / v$$

$$\mathrm{T} = \frac{4\Omega^2 d^4}{v^2} \left(\frac{\eta^2 - \xi}{1 - \psi^2} \right),$$
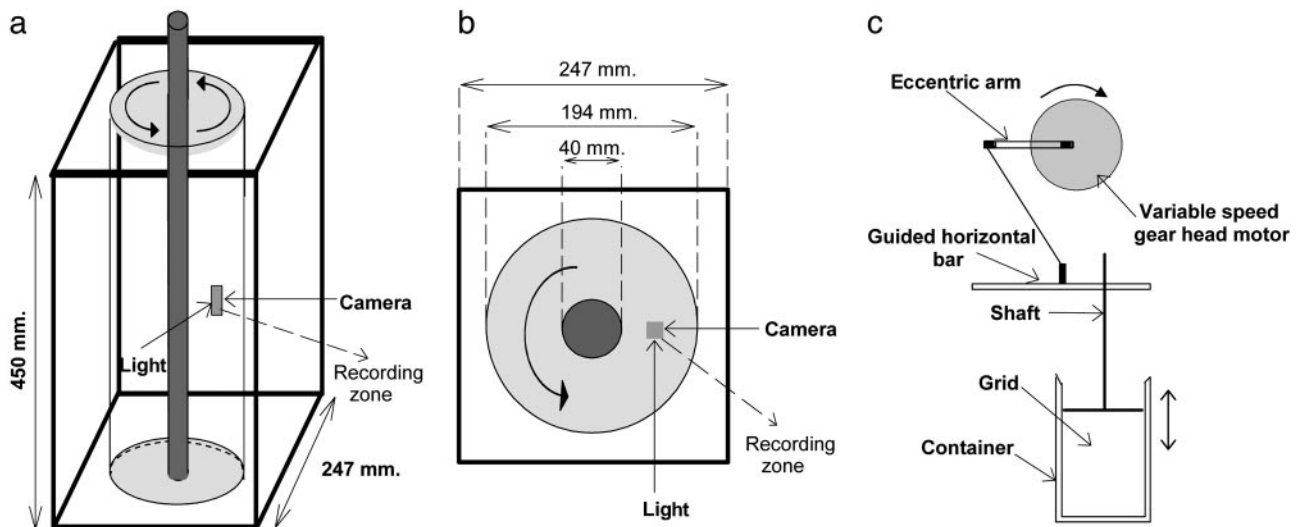
where *r* is the radius of the inner cylinder, *d* is the outer cylinder radius minus *r*, *v* is the kinematic viscosity, and Ψ is *r* divided by the radius of outer cylinder. For those experiments (see below) where the outer cylinder spins in opposite direction to the inner one, ξ is the angular velocity of the outer cylinder divided by Ω.

Fig. 1. Diagram of the rotating (*a* and *b*) and oscillating (*c*) turbulence-generating devices. (*a* and *b*) The whole system was immersed in a water-filled, square-base Plexiglas aquarium. Because the outer cylinder is also Plexiglas, illumination and focus were possible without light or image distortion at a recording zone in a middle point of the annular volume between inner and outer cylinders. The inner spinning system was a PVC cylinder (4-cm diameter). Outer cylinders of different diameters (19, 30, and 114 cm) were implemented and held static in all experiments, except for a case where the 19-cm outer cylinder was spinning in the opposite direction to the inner one. (*c*) Turbulence was generated by means of a vertically oscillating grid in a cylindrical tank 12.9 cm in diameter and 17.2 cm in height. A gearhead motor of variable frequency powered an eccentric arm that vertically moved a guided horizontal bar to which the grid was attached by means of a shaft. The grid was a square mesh of 1.42 cm with bars 0.38 cm in diameter. Velocity measurements were taken 4 and 6 cm below the lowest point of the grid.

Angular velocities and cylinder diameters mentioned above give *Re* and *T* ranging from 3×10^7 to 65×10^7 and from 6,000 to 27,000, respectively. Both ranges indicate a highly unstable and turbulent flow regime (6).

Additional measurements where obtained with very low turbulence levels by stopping the inner cylinder after a period of rotation and then waiting for several minutes before recording sinking velocities. Supplementary Couette experiments were made with the same inner cylinder inside other tanks. The largest tank (114 cm in diameter; annular volume of 520 liters) implemented high angular velocities (up to 9.3 rad per s) to test turbulence under very high Reynolds and Taylor numbers (from 1.7×10^{10} to 76×10^{10} and from 65,000 to 44×10^4, respectively). This experiment was done only with pollen grains owing to the logistic difficulties in producing 500 liters of phytoplankton culture at the concentration needed for optoelectronic recording. The experiment with the smallest tank (19-cm diameter; annular volume of 9 liters) tested the effect on *Coscinodiscus* sp. when the inner and outer cylinders rotated in opposite directions to ensure the total absence of large structures in the flow (7). In addition to the internal *Re* described above, a rotating outer cylinder produces an external *Re*, where *r* and Ω are replaced by the radius and angular velocity of the outer cylinder, respectively. Internal Reynolds numbers ranged from 4,400 to 25,800 and external ones were equal to 9,700, whereas Taylor numbers ranged between 2.3×10^8 and 8.4×10^9 for these experiments with the smallest tank.

Flow visualizations with a Kalliroscope AQ1000 were used to check that the systems described above produce featureless turbulence [*sensu* Andereck *et al.* (7)]. In these conditions, the visible structures in the flow are much smaller than the gap between both cylinders. Therefore, the behavior of particles in the bulk flow away from boundaries is associated with the dynamics of small-scale turbulence and not with large flow structures. This flow state is achieved within 5 min of the start of cylinder rotation. Therefore, for all experiments the cylinder was spun for at least 5 min before starting image acquisition.

Image acquisition was made with a progressive charge-coupled device camera with a matrix of 640×480 pixels. The camera is embedded in a stand-alone machine vision system (VC38, Vision Components, Karlsruhe, Germany) including an onboard processor that carries out the entire image processing described below. To minimize wall effects, the camera was focused from the outside of the tank to a point equidistant from the inner and outer cylinders (Fig. 1 *a* and *b*). A collimated light beam illuminated that point orthogonally to the optical axis of the camera (Fig. 1 *a* and *b*). There was no other illumination source. Therefore, the camera frames a dark field except for the light scattered by suspended phytoplankton that are seen by the system as very bright (white) particles on a black background. The procedure for object detection in machine vision techniques demands a brightness threshold separating the illuminated particle from the background. These highly contrasted images make the process easier. Image processing consisted of thresholding followed by standard segmentation and binarization steps to obtain particle position in the 640×480 matrix of pixels.

One of the short sides (480 rows of pixels) of this rectangular matrix was set in vertical alignment before every experiment. A plumb was hung at the end of a nylon line at the point within the tank focused by the camera. The line could be seen in a monitor connected to the camera, with the vertical sides of the monitor frame corresponding to the 480 pixels sides of the camera. The camera was then slightly rotated around its optical axis to align one of the vertical sides of the monitor with the vertical nylon line. In addition to vertical alignment, the size of the field seen by the camera at the focused point was measured to transform pixels into length units; the factor is 27 μm per pixel.

The camera acquires two consecutive images as fast as possible and stores them in volatile memory, the time lag between acquisitions being 53 ms. A very short lag is necessary to avoid particles leaving or entering the focused field between first and second acquisition. Image processing is not done immediately after each acquisition. Doing so would increase the lag because the camera must wait to process the first image before acquiring a new one. Instead, this computing is done on the stored pair of
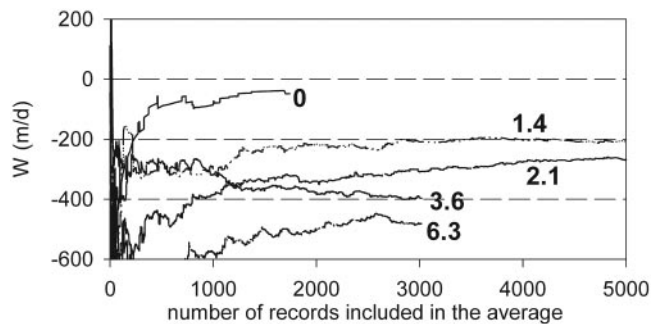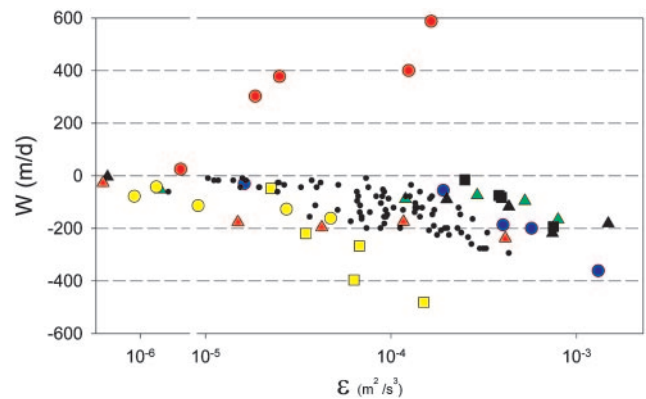
Fig. 2. Mean settling velocity of *Coscinodiscus* sp. (*W*) versus number of records included in the average. *W* progressively reaches an asymptotic value significantly varying for different turbulence intensities. The flow is stationary from the first record. Therefore, this is a statistical and not a flow stabilization process, i.e., a change in the order of the elements which are progressively included in the average produces a similar result. Numbers beside lines indicate the angular velocity of inner cylinder rotation in radians per second. The ANOVA null hypothesis for the asymptotic means has an extremely low probability ($<10^{-10}$).

Fig. 3. *W* versus turbulent kinetic energy dissipation (ε) for all of the experiments. Negative and positive values in the *y* axis are downward and upward velocities, respectively. Symbols for the experiments and the number (given within brackets and ordered according to increasing values of ε) of instantaneous velocity records included in the estimation of *W* are as follows: blue circles, pollen in a 30-cm tank (6,068, 6,951, 10,220, 4,221, and 12,926), inner cylinder rotating and outer cylinder static; yellow circles, pollen in a 114-cm tank (3,006, 2,142, 1,805, 2,475, and 2,516), inner cylinder rotating and outer cylinder static; red circles, *A. salina* cysts in a 30-cm tank (2,098, 6,203, 5,533, 5,881, and 8,339), inner cylinder rotating and outer cylinder static; yellow squares, *Coscinodiscus* sp. in a 30-cm tank (1,742, 8,694, 5,039, 3,020, and 3,017), inner cylinder rotating and outer cylinder static; black squares, *Coscinodiscus* sp. in a 19-cm tank (2,000, 1,250, 3,400, and 1,200), inner cylinder rotating and outer cylinder rotating in opposite direction; black triangles, *Heterocapsa* sp. in a 30-cm tank (3,903, 15,494, 10,879, 11,854, and 10,006), inner cylinder rotating and outer cylinder static; red triangles, *Nitzschia* sp. in a 30-cm tank (7,170, 3,674, 3,019, 8,813, and 7,049), inner cylinder rotating and outer cylinder static; green triangles, *Pleurochrysis* sp. in a 30-cm tank (2,644, 15,921, 7,355, 5,970, and 18,220), inner cylinder rotating and outer cylinder static; black dots, polystyrene beads in the oscillating grid experiment (>6,000 records for each estimation of *W*). Estimated Stokes terminal velocities are of the order of meters per day for *Heterocapsa* sp., *Nitzschia* sp., and *Pleurochrysis* sp. and of the order of tens of meters per day for other particles.

images that have been acquired as fast as possible by the system. The computing time taken to process a pair of images defines the lag between successive pairs and varies from several seconds to several minutes, depending on the number of particles in the images. Therefore, the procedure includes the acquisition and storing of a pair of images in memory (53-ms lag between them), processing of both images to detect particle positions (seconds to minutes), erasing images from memory, acquiring and storing a new pair of images, and so on. Instantaneous vertical velocities are computed during the processing of a pair as the number of rows a particle has moved between consecutive images, multiplied by 27 μm per pixel and divided by 53 ms. The maximum velocity that the system can nominally record is 0.23 m/s (2.0×10^4 m/d). The frequency distribution of velocities is bell-shaped. It is not truncated beyond a certain value and includes records for >10 standard deviations from the mean.

Turbulence intensity was estimated from the standard deviation of the instantaneous vertical velocities (w'). The mechanical and optical design of the system allowed a perfect vertical alignment of the camera frame so that row displacements of particles result, directly, in vertical velocities, as explained above. However, the horizontal axis of the camera frame was neither parallel nor orthogonal to the tank radius. Therefore, column displacements of particles are an unresolved combination of radial and tangential velocities, preventing the use of components different from the vertical in the calculation of turbulent intensity. Thus, the rate of turbulent kinetic energy dissipation (ε) was calculated as (8) $\varepsilon = w'^3/d$, from the standard deviation of one velocity component rather than the fluctuations of the velocity modulus. Because isotropy at small scales makes the three velocity components similar (vertical, radial, and tangential) (8, 6), this is a small underestimation of turbulent intensity and it is not expected to have had a significant effect on the results.

Acoustic: Oscillating grid device. In another set of experiments, a completely different technology was used to generate and to measure turbulence. Turbulence was generated by means of a vertically oscillating grid in a cylindrical tank (Fig. 1c). The tank was made of solid Teflon and had a series of acoustic emitters and receivers mounted flush to the inner wall and aligned to measure three-dimensional particle flow velocities at different points in space by using the Doppler effect. The maximum particle velocity the equipment can nominally register is 2.5 m/s (2.1×10^5 m/d). Signal conditioning and analogue to digital conversion was done with standard electronics for a commercial

acoustic velocimeter (NDV, Nortek AS, Vankrogen, Norway). A solution of NaCl was freshly prepared every day with 0.2 μm of filtered deionized water, for a final salinity of 37, and added to the container. Polystyrene beads 197 μm (±3.9 μm) in diameter and 1.05 g·cm^{-3} were first dispersed in $\approx$20 ml of ethyl alcohol, sonicated, and added to the flow-measuring chamber. The grid was moved with a 4-cm stroke 1 cm below the water surface. Oscillation frequencies ranged from $\approx$0.017 to 0.33 Hz. Particle velocity data were acquired at 25 Hz during $\approx$300 s. The time series was then checked for stationarity of mean and variance, and the mean vertical velocity component (W) was computed. The turbulent kinetic energy dissipation rate was estimated from the $-5/3$ slope range of the energy spectrum of *w*, using the linear regression method (9).

Results

The mean velocity (W) obtained with the intelligent camera for *Coscinodiscus* sp. at different turbulence levels as a function of the number of records is shown in Fig. 2. Random fluctuations imposed by turbulence demand a large number of records before the mean velocity reaches a stable value. The surprising feature is that these asymptotic mean values are not the same for the different turbulence intensities tested. *A priori*, no changes in W would be expected from the superposition of a zero mean noise (resulting from turbulence isotropy at small scales) on a deterministic settling velocity (resulting from density differences between *Coscinodiscus* sp. and water).

Turbulence increases the mean settling velocity in all cases (Fig. 3), in opposition to inductive expectations. It is a significant

Fig. 4. *W* of *A. salina* cysts versus salinity. The experiment implemented the 19-cm-diameter tank, static outer cylinder, and the inner cylinder rotating at 3 rad/s. The turbulent kinetic energy dissipation rate is of the order of 3×10^{-4} $m^2 \cdot s^{-3}$ for all salinities. The thick line represents the estimated Stokes terminal velocity.

Fig. 5. Absolute value of *W* versus ESD/η for all of the experiments.

increase when turbulence shifts from the low values to the higher values recorded in upper mixed layers (10, 11). This process affects all species as well as the inert pollen and polystyrene particles and occurs independently of the turbulence system and of the velocity recording device implemented. Therefore, this persistent effect cannot result from an experimental artifact and must arise from particle interaction with the turbulent flow. Contrary to particles denser than seawater, the floating *A. salina* cysts increase their upward velocity under higher turbulence levels. This finding leads us to consider that this effect emerges from the dynamics of particles similar in size to phytoplankton when immersed in a turbulent flow under the influence of gravitational forces. Turbulence enhances the downward or upward velocities of particles that settle or float, respectively, in still fluid. Because cysts are immersed in a range of salinity-manipulated water under otherwise constant experimental conditions and turbulence levels (Fig. 4), the effect on vertical particle velocity is well beyond that expected from Stokes terminal velocity and is further evidence for this interpretation.

Modeling analysis of turbulent fluid dynamics backs up this hypothesis because settling particles do not sink along a straight path when vortical structures are present (12, 13). Instead, simulations predict that the complex interaction of gravitational forces, added mass effects, pressure gradients, and viscous forces acting on a settling particle in a turbulent flow make particle populations diverge out from regions of high vorticity and converge preferentially in regions of low vorticity and high strain rate, and with the same flow direction as the gravity force (13, 14). As a result, the spatial distribution of settling particles in a turbulent flow is not random, and preferential concentration occurs in the downward moving section of eddies' peripheries (13). Nonrandom distribution of particles is a clear feature in the visualization of these simulations (15). Additional experimental evidence for the hypothesis could come from the empirical verification of these nonrandom distributions for phytoplankton by means of imaging techniques, not available yet, capable of resolving the individual position of a large number of cells in a turbulent flow.

On average, preferential concentration adds a new downward component to the sinking velocity of phytoplankton cells settling in a turbulent flow with respect to still water. A symmetric upward case applies to floating particles like *A. salina* cysts. Our results are in line with this hypothesis, especially for the larger

particles in the experiment: *Coscinodiscus* sp. cells, polystyrene spheres, and *A. salina* cysts. Their vertical velocities are very sensitive to high turbulence, unlike the magnitude of their fluctuating velocity. This feature might reflect a probabilistic tendency to preferentially reside in the downward (*Coscinodiscus* sp., polystyrene) or upward (cysts) flows among the smallest eddies.

Thus, particles would have a smaller fluctuating component than if they were randomly alternating between downward and upward flows during settlement. An additional element supporting this model is the fact that, as expected by the hypothesis of Wang and Maxey (13), *W* varies with the ratio of particle size to the size of the smallest eddies and is sensitive to the Stokes number of particles (Fig. 5). Preferential concentration is more intense when particle size is similar to the Kolmogorov microscale $(\nu^3/\varepsilon)^{1/4}$, where ν is kinematic viscosity (13, 14). This is evident in Fig. 5, where *W* increases as the ratio ESD/η approaches the value 1 for each experiment. The ratio of length scales between particles and flow is not the unique factor affecting particle settling and preferential concentration in a turbulent flow. These dynamics are also sensitive to the ratio of time scales between particles and flow (13–15), which is contained in the Stokes number, $18 \rho_w \nu^{3/2} \Delta\rho ESD^2 \varepsilon^{1/2}$ (where ρ_w is the density of seawater and $\Delta\rho$ is the difference of density between particles and seawater, assumed to be 0.1 $g \cdot cm^{-3}$ in these calculations). The Stokes number varies as the square of particle diameter. This dependence magnifies the size differences among the particles we used in the experiments and generates the two clouds in Fig. 5. One cloud contains particles with ESD of the order of hundreds of micrometers (*Coscinodiscus sp.*, polystyrene spheres, and cysts) resulting in a median Stokes number of 5×10^{-3}. The other cloud contains particles with ESD of the order of tens of micrometers and a median Stokes number of 10^{-4}, 50 times smaller.

Regardless of the mechanical details, *W* increases when phytoplankton cells are subjected to naturally occurring turbulence intensities. Settling causes phytoplankton to leave the upper mixed layer through the bottom boundary as a sedimentation flux equal to WC_B, with C_B being the cell concentration at the bottom of the layer (16). The rate of phytoplankton sedimentation resulting from this flux is usually modeled as WC_B/H, where *H* is the mixed layer depth (16, 17). Therefore, the overall effect of turbulence on phytoplankton sedimentation rate out from mixed layers stems from the net balance of these three elements. Turbulent modifications of C_B are negligible for the vast majority of phytoplankton species and turbulence conditions of upper mixed layers (18). Lake experiments where plastic

bags are used to generate a gradient of mixing depths clearly reveal a decrease of phytoplankton sedimentation with increasing H (19). At the ocean surface, high turbulence usually results in deep (hundreds of meters) mixed layers with respect to calm conditions (tens of meters), therefore modifying H by a factor of ≈ 10. This change is similar to the expected rise in W when turbulence shifts from low to high values (Fig. 3) and probably implies that the overall direct effect of turbulence on the sedimentation rate of phytoplankton is close to null. Additional indirect effects might arise as a result of the formation/break-up of phytoplankton aggregates with a large size under different turbulent regimes (20), from modifications in cell buoyancy associated with nutrient enrichment when H increases (21), or from population dilution when entrainment introduces deep water that is poor in cells into the surface.

This direct effect for upper mixed layers of lakes and oceans is in apparent contradiction with the usual observations of particles that tend to resuspend when in turbulent flows. The discrepancy is only apparent and does not result from particle dynamics in the bulk flow but from differences in the nature of bottom boundaries. Thus, Fig. 3 clearly shows an increase of W in the bulk flow when turbulence intensifies, although phytoplankton did not accumulate at the bottom of the experiments with rotating cylinders. High W in the bulk flow and no phytoplankton accumulation at the bottom are compatible because the proximity of this solid boundary cancels downward, but not upward, particle motion. This asymmetry allows the particles to remain at the bottom boundary until they are recovered by a strong upward turbulent fluctuation and immersed again in the bulk flow, where they can again have a high W. In fact, a solid bottom involves complex interactions among the particles, the fluid, and the boundary surface, which are controlled by factors like particle shape or surface roughness (22, 23). These interactions force particle concentration (24) and might reduce gravitational settling (23). However, the pycnocline at the bottom of the mixed layer of lakes and oceans is not solid. Contrary to solid boundaries, the asymmetry for particle sedimentation does not occur for pycnoclines, and particles do not remain at this boundary until recovered into the bulk flow by turbulence.

Therefore, increased turbulence in the mixed layer increases W but cannot recover particles from the pycnocline. This is a paradoxical situation, because it implies that turbulence can never reverse the sedimentation of phytoplankton from surface mixed layers. Thus, if nonmotile phytoplankton cannot rely on turbulence, how can they remain at surface layers for generation after generation? For cases where phytoplankton abundance is actually higher below the mixed layer, entrainment results in a net upward transport of cells. When this is not the case, fluid dynamics at scales larger than those associated with isotropic turbulence must have a relevant role in maintaining phytoplankton in the photic zone. For instance, upward flows associated with mesoscale events can balance the sinking of larger and heavier cells (25). In the absence of these events, compensatory physiological mechanisms, such as those described for diatoms that are able to decrease their density when in unlit waters (26), may partly facilitate the use of deep-water nutrients (27) and also help avoid the population sinking in an environment where turbulence is unable to prevent settling if cells are denser than water. In light of our results, turbulent energy must be considered as an additional handicap to be overcome by phytoplankton aiming to avoid sedimentation. This conclusion challenges the classical view of turbulence as a positive environmental element that prevents phytoplankton from sinking from the surface to depth.

1. Arin, L., Marrasé, L., Maar, M., Peters, F., Sala, M.-M. & Alcaraz, M. (2002) *Aquat. Microb. Ecol.* **29,** 51–61.
2. Saiz, E. & Kiørboe, T. (1995) *Mar. Ecol. Prog. Ser.* **122,** 147–158.
3. Berdalet, E. (1992) *J. Phycol.* **28,** 267–272.
4. Ramaswamy, S. (2001) *Adv. Phys.* **50,** 297–341.
5. Peters, F. & Redondo, J. M. (1997) *Sci. Mar.* **61,** 205–228.
6. Tritton, D. J. (1988) *Physical Fluid Dynamics* (Oxford Univ. Press, Oxford).
7. Andereck, C. D., Liu, S. S. & Swinney, H. L. (1986) *J. Fluid Mech.* **164,** 155–183.
8. Tennekes, H. & Lumley, J. L. (1972) *A First Course in Turbulence* (MIT Press, Cambridge, MA)
9. Stiansen, J. E. & Sundby, S. (2001) *Sci. Mar.* **65,** 151–167.
10. Brainerd, K. E. & Gregg, M. C. (1993) *J. Geophys. Res.* **98,** 22645–22656.
11. Saggio, A. & Imberger, J. (2001) *Limnol. Oceanogr.* **46,** 392–409.
12. Werely, S. T. & Lueptow, R. M. (1999) *Phys. Fluids* **11,** 325–333.
13. Wang, L.-P. & Maxey, M. R. (1993) *J. Fluid Mech.* **256,** 27–68.
14. Vaillantcourt, P. A. & Yau, M. K. (2000) *Bull. Am. Meteorol. Soc.* **81,** 285–298.
15. Squires, K. D. & Yamazaqui, H. (1995) *Deep-Sea Res. II* **42,** 1989–2004.
16. Ruiz, J. (1996) *J. Mar. Res.* **54,** 385–406.
17. O'Brien, K. R., Ivey, G. N., Hamilton, D. P. & Waite, A. (2003) *Limnol. Oceanogr.* **48,** 1326–1337.
18. Ruiz, J., García, C. M. & Rodríguez, J. (1996) *J. Plankton Res.* **18,** 1727–1734.
19. Ptacnik, R., Diehl, S. & Berger, S. (2003) *Limnol. Oceanogr.* **48,** 1903–1912.
20. Ruiz, J. (1997) *Deep-Sea Res.* **44,** 1105–1126.
21. Villareal, T. A., Altabet, M. A. & Culver-Rymsza, K. (1993) *Nature* **363,** 709–712.
22. Zang, H., Ahmadi, G., Fan, F.-G. & McLaughlin, J. B. (2001) *Int. J. Multiphase Flow* **27,** 971–1009.
23. Sommerfeld, M. & Huber, N. (1999) *Int. J. Multiphase Flow* **25,** 1457–1489.
24. Wang, J. & Levy, E. K. (2003) *Exp. Thermal Fluid Sci.* **27,** 845–853.
25. Rodríguez, J., Tintoré, J. T., Allen, J. T., Blanco, J. M., Gomis, D., Reul, A., Ruiz, J., Rodríguez, V., Echevarría, F. & Jiménez-Gómez, F. (2001) *Nature* **410,** 360–363.
26. Bienfang, P., Szyper, J. & Laws, E. (1983) *Oceanol. Acta* **6,** 55–62.
27. Villareal, T. A., Pilskaln, C., Brzezinski, M., Lipschultz, F., Dennett, M. & Gardner, G. B. (1999) *Nature* **397,** 423–425.